International Journal of Modern Physics B
Vol. 32, No. 31 (2018) 1850350 (9 pages)

DOI: 10.1142/S0217979218503502

The stability of graphene-based Möbius strip with vacancy and at high-temperature

Kaishuai Yang*,†, Chuanguo Zhang*,†, Xiaohong Zheng*,†,
Xianlong Wang*,†,‡,¶ and Zhi Zeng*,†,§,¶

*Key Laboratory of Materials Physics,
Institute of Solid State Physics,
Chinese Academy of Sciences, Hefei 230031, P. R. China
†University of Science and Technology of China,
Hefei 230026, P. R. China
‡xlwang@theory.issp.ac.cn
§zzeng@theory.issp.ac.cn

Received 16 July 2018
Revised 4 October 2018
Accepted 18 October 2018
Published 19 December 2018

The structural and electronic properties of mono-vacancy (MV) defect in graphene-based Möbius strip (GMS) are studied in the framework of density functional theory (DFT) combined with the molecular dynamics (MD) simulations. Two kinds of MV defects are observed: the 59-type MV (a configuration with one pentagon and one nonagon ring) located at the curved areas of Möbius strip, and the 5566-type MV (a configuration with two pentagon and two hexagon rings) with one sp^3 hybridized carbon appeared in the twisted areas. The 5566-type MV defect is the most stable configuration at 0 K, while the DFT-MD calculations show that it is unstable at room-temperature and will transform into a 59-type MV. Additionally, the melting behavior of GMSs is investigated through empirical potential MD simulations, and we find that their melting temperatures are about 2750 K, which is lower than that of carbon nanotubes and graphene.

Keywords: Graphene-based Möbius strip; mono-vacancy defect; melting temperature.

PACS numbers: 61.48.De, 61.48.Gh, 61.72.Ji

1. Introduction

The graphene-based Möbius strip (GMS) has attracted extensive attentions due to its special topological property, one face and one edge, which makes it distinct from other carbon-based low-dimensional materials, such as carbon nanotubes and graphene. Möbius aromatic hydrocarbon had been successfully synthesized in

¶Corresponding authors.

experiments,[1,2] while the GMS has not been experimentally synthesized yet. Moreover, theoretical simulations focused on the properties of GMS heavily, since it may have important applications.[3–11] The simulated results demonstrate that GMS is a stable structure,[9] and show novel optical[4,10] and magnetic properties.[6,10] Especially, it is also believed to be a topological insulator.[7] In our previous work,[9] the structural configurations of GMS with different ratios between length and width are presented, and we find that since GMS has only one edge, differing from graphene nanoribbons, ferromagnetic state is the ground state of GMS.

Carbon-based materials are usually not ideal crystals, and atomic vacancies can affect their properties significantly,[12–21] for example, inducing magnetism in graphene.[13,15] Previous works focused heavily on the properties of atomic vacancies presented in carbon nanotubes and graphene,[12–15,17–30] where atomic vacancies can be introduced unintentionally during the processes of synthesis or deliberately by irradiation, chemical, and plasma treatments. Among different types of atomic vacancies in carbon nanostructures, mono-vacancy (MV) with one atom missing from lattice is a simple, popular, and attractive one, and it has been identified clearly by experimentalists and theorists in carbon nanotubes and graphene.[15,29–32] In these systems, MV undergoes a Jahn–Teller distortion, which leads to the formation of covalent bond between two of three atoms located around the atomic vacancy resulting in one five-membered ring and one nine-membered ring (59-type MV). To date, only 59-type MV was reported in carbon nanotubes and graphene.

In order to fully understand the GMS, it is important and necessary to illustrate the MV properties in GMS. First of all, the structural configurations of the MV in the GMS should be clarified. As shown in our previous work,[9] since each GMS is composed by two kinds of areas, curved and chiral twisted parts, the MV features in GMS should be investigated separately depending on its local structures. In this work, based on the first-principles method, the structural and electronic properties of the MV in GMS are investigated. Our results show that besides 59-type MV present in the curved area, a 5566-type MV, which has two pentagons and two hexagons and acquires one sp^3 carbon atom at the central site, is observed in the twisted region. To the best of our knowledge, the 5566-type MV is not reported in carbon-based low-dimensional materials. Furthermore, due to the strain introduced by their edges, graphene nanoribbons with chiral twist were theoretically predicted,[33–37] and in fact experimentally observed.[38] The shapes of graphene nanoribbons with different chiral twisted degrees were clearly shown by transmission electron miscroscopy (TEM) images.[39] Furthermore, graphene nanoribbons can transform into carbon nanotubes through chiral twisting,[40] and the local configurations of the twisted areas of GMS are similar to that of graphene nanoribbons with chiral twisting. Therefore, the explored MV behaviors of present work can also be used to analyze the properties of chirally twisted carbon nanotubes and graphene. Furthermore, the melting temperature of GMSs with different ratios between length and width is illustrated.

2. Computational Methods

The calculations are performed by the SIESTA package, in which the norm-conserving pseudopotential and linear combinations of atomic orbital basis sets are used.[41,42] The wave function is expanded with double-ζ (DZ) basis sets, and the exchange-correlation potential of generalized gradient approximation (GGA) with the form of Perdew–Burke–Ernzerhof (PBE) is selected.[43] The lattice vectors ($50 \times 50 \times 50$ Å) are large enough to avoid the interactions from adjacent neighbors. All related structures are fully relaxed. The method and parameters used in this work are basically the same as that in our previous works.[9,44] The melting behaviors of GMSs are investigated via MD simulations using the LAMMPS[45] and Adaptive Intermolecular Reactive Empirical Bond Order (AIREBO) Potential[46] for a system of carbon and hydrogen atoms with the LJ cutoff 3.0 Å. The configurations of GMSs are relaxed under a series of Nose–Hoover thermostat[46,47] from 1000 K to 3500 K for 6.25×10^6 steps with a time step of 0.5 fs.

3. Results and Discussion

In our previous work,[9] the structural features and formation energies of GMS as a function of width-to-length ratio are illustrated. We find that one, two and three planar triangle regions can be observed in GMS, and their formation energies increase with the ratio of width-to-length increasing. Following, we will use n–m to represent the GMS structures, where n and m indicate the length (numbers of armchair lines) and the width (numbers of zigzag lines) of GMS, respectively. For example, 30–06 means the GMS with the length of 30 armchair lines and the width of 6 zigzag lines, which contains one planar triangle area, as shown in Fig. 1(a). Because of its topological property, GMS can be separated to three different areas depending on local deformation. As shown in Fig. 1(a), A and C denote the areas with twisting, while B is the curved area similar to carbon nanotubes. One carbon atom in the central site of A, B and C areas is removed to generate the initial structure of MV, and these MVs are hereafter denoted as MV-A, MV-B and MV-C, respectively. After fully structural relaxations at 0 K, the relaxed structures of MV-A, MV-B and MV-C are shown in Figs. 1(b), 1(c) and 1(d), respectively, and the zoomed in views are presented in the corresponding insets to clearly illustrate their structures. The formation energy (Ω) of MV in GMS (labeled as ΩMV (GMS)) and graphene (labeled as ΩMV (G)) are given by the following equations:

$$\Omega_{\mathrm{MV}}(\mathrm{GMS}) = E_{\mathrm{MV}}(\mathrm{GMS}) + E_{\mathrm{atom}} - E(\mathrm{GMS}), \tag{1}$$

$$\Omega_{\mathrm{MV}}(G) = E_{\mathrm{MV}}(G) + E_{\mathrm{atom}} - E(G), \tag{2}$$

$$E_{\mathrm{atom}} = E(G)/N, \tag{3}$$

where E(GMS) (E(G)) and E_{MV} (GMS) (E_{MV}(G)) denote the total energies of GMS (graphene) without and with MV, respectively, and N is the number of carbon atoms in a 12×12 graphene supercell. The calculated results are presented in

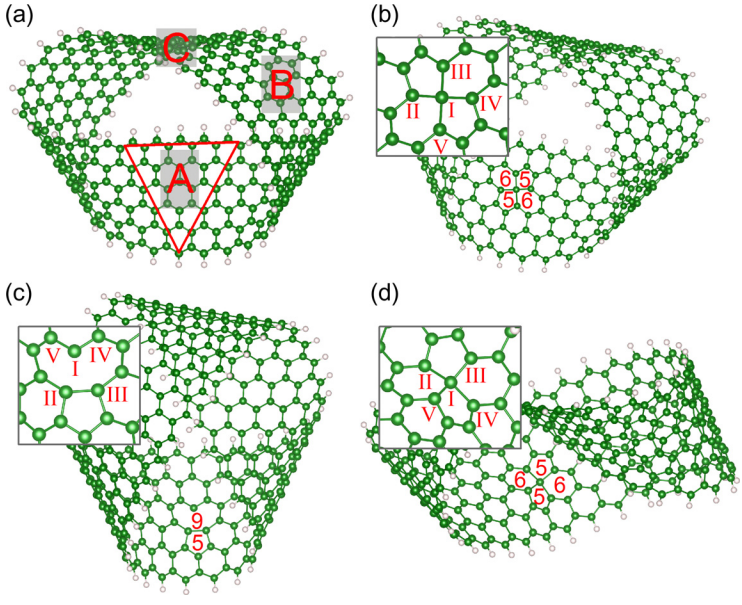

Fig. 1. (Color online) (a) The structure of ideal Möbius strip, and A, B and C are used to present the areas to create MV. Red triangle shows the planar area. (b), (c), and (d) show the relaxed structures of MV introduced in the A (MV-A), B (MV-B) and C (MV-C) areas, respectively, while the enlarged structures are presented in the insets. The arabic numbers presented in figures are used to indicate the configurations of MV. The greek numbers presented in insets are used to indicate the atomic sites of MV.

Table 1. Formation energies of mono-vacancies at 0 K.

eV	Graphene	MV-A (5566)	MV-B (59)	MV-C (5566)
Formation energy	7.56	6.43	6.51	6.72

Table 1, the formation energy of MV in graphene is 7.56 eV, which agrees well with that of the published results (7.4 eV[32] and 7.7 eV[15]), indicating that our used method and parameters can sufficiently describe graphene. The formation energies of MV-A, MV-B and MV-C are 6.43 eV, 6.51 eV and 6.72 eV, respectively. The MV formation energies of GMS are about 1 eV smaller than that of graphene (7.56 eV). The results show that compared with infinite graphene, it will be easier to introduce MVs in GMS or graphene with chiral twisting partially due to the existence of strain. Furthermore, as shown in Table 1, the most stable MV is the MV-A, which has the smallest formation energy and locates at the planar triangle area (A area). The structural properties of MV-A, MV-B, and MV-C are listed in Table 2.

As can be found in Fig. 1(c), MV-B shows a typical 59-type pattern with one pentagon and one enneagon similar to that in carbon nanotubes and graphene.[15,31,32] A new bond is formed between atom II and atom III with the

Table 2. Structural properties of MV-A, MV-B, and MV-C. Distance (d) and angle (a) are shown in the unit of Å and degree, respectively.

	$d_{\mathrm{I-II}}$	$d_{\mathrm{I-III}}$	$d_{\mathrm{I-IV}}$	$d_{\mathrm{I-V}}$	$a_{\mathrm{II-I-IV}}$	$a_{\mathrm{III-I-V}}$	$a_{\mathrm{II-I-III}}$	$a_{\mathrm{II-I-V}}$
MV-A	1.62	1.67	1.60	1.68	138.0	147.6	96.2	96.1
MV-B	2.57	2.55	1.39	1.40	125.8	128.6	35.9	94.4
MV-C	1.61	1.69	1.60	1.68	138.1	145.7	96.3	96.1

Table 3. The magnetic moments and electric charge of carbon atoms located at the edge and central site of perfect Möbius strip and with MV-A, MV-B and MV-C defect using Mülliken analysis, respectively. The values of edge carbon atoms closest to the central site of MV defects are presented.

	Magnetism (μ_B)		Charge (e)	
Configuration	Edge	Center	Edge	Center
MV-A	0.234	0.001	3.808	3.937
MV-B	0.244	0.585	3.806	4.089
MV-C	0.240	0.002	3.808	3.936
Perfect	0.224	−0.009	3.820	3.987

bond-length of 1.59 Å, which is much shorter by 0.98 Å than the distance (2.57 Å) between atom I and atom II (seen in Table 2), due to the Jahn–Teller distortion. Furthermore, the distances between atom I and its neighbors (atom IV and atom V) in MV-B are about 1.40 Å, shorter than the C–C bond in graphene (1.42 Å), since the atom I in MV-B just has two nearest neighbors, which also cause the largest electronic charge (4.089 e) and magnetic moment (0.585 μ_B) of the atom I in MV-B shown in Table 3. Interestingly, after structure relaxations, MV-A and MV-C in the twisted areas evolve into a novel 5566-type pattern with two kinds of bond angles ($\sim$96° and $\sim$140°, shown in Table 2), which is different from that of graphene (sp^2-type hybridization with 120° bond angle). In the cases of MV-A and MV-C, the average distance between the central carbon atom and its four neighbors is about 1.64 Å, which is larger than the C–C bond-length (1.42 Å) of graphene and the new bond formed in MV-B (1.59 Å) and diamond (1.55 Å). Combined with the bond-angle information of MV-A to MV-C shown in Table 2, we can conclude that the carbon atoms located at their central sites are of a sp^3 type.

To further prove the sp^3-type hybridization from the point of electronic structures, the partial density of states (PDOS) of atom at the edge and at the central site of the ideal planar triangle area in GMS are presented in Figs. 2(a) and 2(b), respectively. Meanwhile, the PDOS of the central carbon atom in 5566-type and 59-type MV is presented in Figs. 2(c) and 2(d), respectively. If we compare Fig. 2(b) with Fig. 2(c), the energy gap around the Fermi level shown in Fig. 2(c) is much larger than that of sp^2 hybridized carbon in Fig. 2(b), indicating that the central carbon atom of MV-A and MV-C hybridize with its four neighbors by sp^3-like bonding.

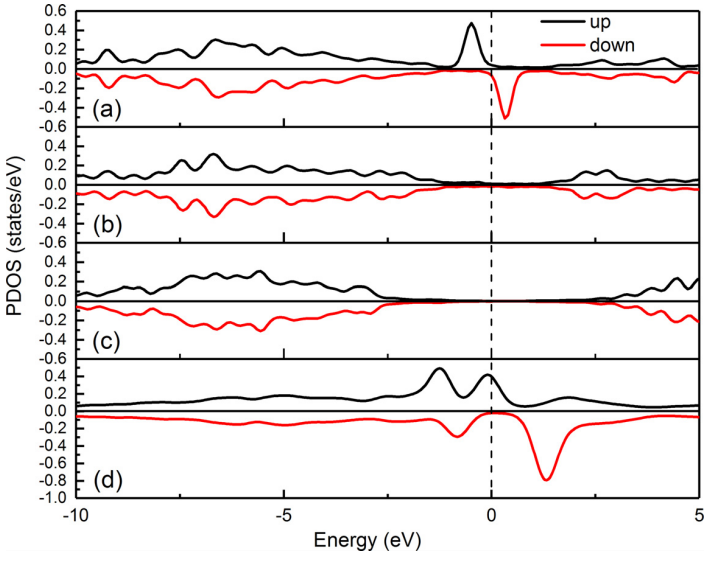

Fig. 2. (Color online) The partial density of states (PDOS) of carbon atom located at the edge site of perfect Möbius strip (a), the central site of planar triangle area of perfect Möbius strip (b), the central site of MV-A (c) and the central site of MV-B (d).

The magnetic moments and electronic charges of carbon atoms in GMS with and without MV are summarized in Table 3. The carbon atom at the edge site of pure GMS is spin polarized with a magnetic moment of 0.224 μ_B similar to the case of graphene nanoribbons with zigzag edge and agrees with previous work,[9,44] which consist with the corresponding PDOS profile shown in Fig. 2(a). The sharp peaks around the Fermi level can be found in the PDOS of carbon at edge site, and the spin polarization origins from the p_z orbital. Since the carbon atom at the central site has the sp^3-type hybridization, the 5566-type MV (MV-A and MV-C) does not have spin polarization. Moreover, because of the dangling sigma bond, the magnetic moment of carbon atoms at the central site of MV-B (59-type MV) is as high as 0.585 μ_B, which is similar to that in graphene and nanotubes.[13,15] The large spin polarization of carbon atoms at the central site of MV-B can be found in the PDOS of Fig. 2(d). From Table 3, we can find that whether introducing 5566-type or 59-type MV in GMS, the magnetic moments of edge carbon atoms near the MVs are about 0.240 μ_B, comparing to that of perfect GMS (0.224 μ_B). The results indicate that the spin polarization of carbon atoms at edge in GMS is tough and not sensitive to the MV. Therefore, the ferromagnetic coupling along GMS edges[9] is also not sensitive to the MVs.

So far, two 5566-type MV (MV-A and MV-C) and one 59-type MV (MV-B) are obtained at 0 K based on the structural relaxations, and temperature effects are not included. Following, we will discuss the stability of 5566-type MV-A at room-temperature, which is the most stable MV configuration at 0 K. For this purpose, DFT-MD simulations of MV-A at room-temperature (T = 300 K) are

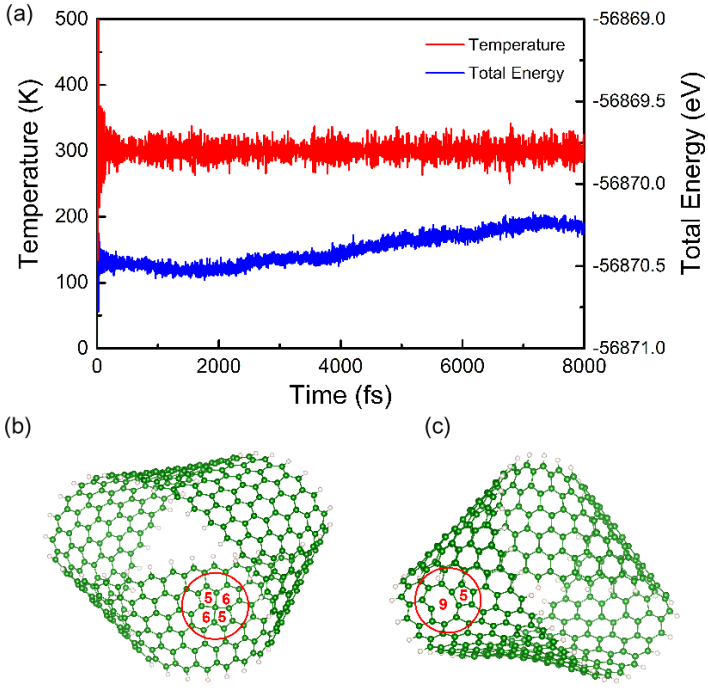

Fig. 3. (Color online) (a) Temperature and total energy as a function of time obtained from molecular dynamics simulation. (b) and (c) present the *initio* (5566-type MV) and final (59-type MV) configuration before and after running the molecular dynamics simulation.

done in the time step of 1 fs, and the corresponding results are shown in Fig. 3(a). After running 8000 DFT-MD steps, we find that the 5566-type MV-A [shown in Fig. 3(b)] will transform into a 59-type MV-B pattern [shown in Fig. 3(c)]. The result shows that the 5566-type defect can only exist at low-temperature, and it is not a stable configuration at room-temperature. In other words, the 5566-type MV may contribute sp^3-type spectral signals in the carbon-based low-dimensional materials with chiral twisting at low-temperature condition. At room-temperature, the 5566-type defect will undergo an immigration from the twisting area A to the curved area B, meanwhile turning into a 59-type defect. Similar scenario may also occur in other low-dimensional materials, such as carbon nanotubes and graphene.

Even though the melting temperature of graphene (∼4500 K)[48] and carbon nanotubes (∼3100 K)[49] are known, the melting temperature of GMS is still not clarified yet. The melting temperature of GMS is one of the important parameters for its potential applications. To investigate the melting temperature of GMS, five different GMS configurations (30–06, 30–08, 30–10, 30–12, 30–14) with different widths are investigated. As shown in Fig. 4, the internal energies of these GMSs have a sharp increase when the temperature increases to a certain value. The dramatic changes of internal energy are clear signal for the larger structural changes. We define the temperature, where the internal energies increase dramatically, as the

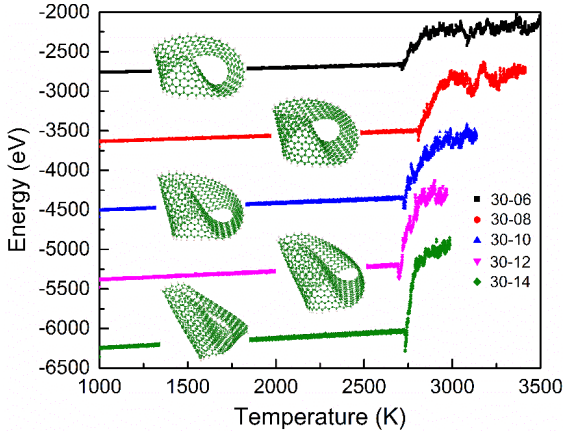

Fig. 4. (Color online) Internal energies of Möbius strips numbered by 30–06, 30–08, 30–10, 30–12 and 30–14 are shown in the black, red, blue, pink and green lines, respectively. The structures of the Möbius strips are shown in the corresponding insets.

melting point. All investigated GMSs have comparable melting temperatures of ∼2750 K, because the melting point is mainly determined by the materials' bonding property and internal stress. The melting temperature of GMS is much lower than that of graphene (∼4500 K)[48] and carbon nanotubles (∼3100 K).[49]

4. Conclusions

The structural and electronic properties of MV in Möbius strip formed from graphene are simulated based on the DFT. The 5566-type MV with a sp^3 hybridized carbon atom at central site is observed in the chiral twisted areas of GMS, while a 59-type MV appears in the curved area. Though the 5566-type MV has the lowest energy at 0 K, our DFT-MD simulations show that the 5566-type MV is not stable at room-temperature, and it will transform into a 59-type MV, the similar scenario may occur in other low-dimensional materials, e.g., carbon nanotubes. Additionally, the melting temperature of GMSs is about 2750 K, which is lower than that of carbon nanotubles and graphene.

Acknowledgments

This work was supported by the National Natural Science Foundation of China under Grant Nos. 11674329, 11605231 and 11574318, Science Challenge Project, No. TZ2016001. The calculations were partly performed in Center for Computational Science of CASHIPS.

References

1. D. Ajami *et al.*, *Nature* **426**, 819 (2003).
2. R. P. John *et al.*, *J. Am. Chem. Soc.* **129**, 14142 (2007).

3. J. Gravesen and M. Willatzen, *Phys. Rev. A* **72**, 032108 (2005).
4. N. Zhao *et al.*, *Phys. Rev. B* **79**, 125440 (2009).
5. D. J. Ballon and H. U. Voss, *Phys. Rev. Lett.* **101**, 247701 (2008).
6. D.-E. Jiang and S. Dai, *J. Phys. Chem. C* **112**, 5348 (2008).
7. Z. L. Guo *et al.*, *Phys. Rev. B* **80**, 195310 (2009).
8. J. W. Jiang, J. S. Wang and B. Li, *Europhys. Lett.* **89**, 46005 (2010).
9. X. Wang *et al.*, *Appl. Phys. Lett.* **97**, 123103 (2010).
10. Z. Li and L. R. Ram-Mohan, *Phys. Rev. B* **85**, 195438, (2012).
11. J. Kreismann and M. Hentschel, *Europhys. Lett.* **121**, 24001 (2018).
12. P. Esquinazi *et al.*, *Phys. Rev. Lett.* **91**, 227201 (2003).
13. M. M. Ugeda *et al.*, *Phys. Rev. Lett.* **104**, 096804 (2010).
14. V. M. Pereira *et al.*, *Phys. Rev. Lett.* **96**, 036801 (2006).
15. Y. Ma *et al.*, *New J. Phys.* **6**, 68 (2004).
16. M. Ichida *et al.*, *Solid State Commun.* **250**, 119 (2017).
17. D. Teich, M. Claus and G. Seifert, *J. Comput. Electron.* **17**, 521 (2018).
18. X. Li *et al.*, *Carbon* **133**, 186 (2018).
19. A. J. M. Giesbers *et al.*, *Solid State Commun.* **229**, 49 (2016).
20. S. Ebrahimi, *Solid State Commun.* **220**, 17 (2015).
21. W. L. Scopel, W. S. Paz and J. C. C. Freitas, *Solid State Commun.* **240**, 5 (2016).
22. L. Tapasztó *et al.*, *Phys. Rev. B* **78**, 233407 (2008).
23. D. Teweldebrhan and A. A. Balandin, *Appl. Phys. Lett.* **94**, 013101 (2009).
24. F. Banhart, J. Kotakoski and A. V. Krasheninnikov, *ACS Nano* **5**, 26 (2011).
25. G. Eda, G. Fanchini and M. Chhowalla, *Nat. Nanotechnol.* **3**, 270 (2008).
26. H. Wang *et al.*, *J. Am. Chem. Soc.* **131**, 9910 (2009).
27. A. Hansson, M. Paulsson and S. Stafström, *Phys. Rev. B* **62**, 7639 (2000).
28. G. D. Lee *et al.*, *Phys. Rev. Lett.* **95**, 205501 (2005).
29. J. Kotakoski *et al.*, *Phys. Rev. Lett.* **106**, 105505 (2011).
30. A. Hashimoto *et al.*, *Nature* **430**, 870 (2004).
31. K. Kim *et al.*, *Nano Lett.* **8**, 3092 (2008).
32. A. A. El-Barbary *et al.*, *Phys. Rev. B* **68**, 144107 (2003).
33. B. V. Martins and D. S. Galvao, *Nanotechnology* **21**, 75710 (2010).
34. V. B. Shenoy *et al.*, *Phys. Rev. Lett.* **101**, 245501 (2008).
35. K. V. Bets and B. I. Yakobson, *Nano Res.* **2**, 161 (2010).
36. H. Wang and M. Upmanyu, *Phys. Rev. B* **86**, 205411 (2012).
37. Y. Li, *J. Phys. D: Appl. Phys.* **43**, 495405 (2010).
38. X. Li *et al.*, *Science* **319**, 1229 (2008).
39. T. W. Chamberlain *et al.*, *ACS Nano* **6**, 3943 (2012).
40. O. O. Kit *et al.*, *Phys. Rev. B* **85**, 085428 (2012).
41. J. M. Soler *et al.*, *J. Phys.: Condens. Matter* **14**, 2745 (2002).
42. P. Ordejón, *Physica Status Solidi(b)* **217**, 335 (2000).
43. J. P. Perdew, K. Burke and M. Ernzerhof, *Phys. Rev. Lett.* **77**, 3865 (1996).
44. X. H. Zheng *et al.*, *Phys. Rev. B* **86**, 081408 (2012).
45. S. Plimpton, *J. Comput. Phys.* **117**, 1 (1995).
46. W. G. Hoover, *Phys. Rev. A* **31**, 1695 (1985).
47. W. G. Hoover, *Phys. Rev. A* **34**, 2499 (1986).
48. J. H. Los *et al.*, *Phys. Rev. B* **91**, 045415 (2015).
49. P. G. Collins and P. Avouris, *Sci. Am.* **283**, 62 (2000).